Electronic Supplementary Information

Reactivity of *N*–heterocyclic carbene–pyridine palladacyclopentadiene complexes toward halogens addition. The unpredictable course of the reaction

F. Visentin, T. Scattolin, C. Santo, N. Demitri and L. Canovese

[a] *Dipartimento di Scienze Molecolari e Nanosistemi, Università Ca' Foscari, Venice, Italy.*
E. Mail: cano@unive.it

[b] Elettra – *Sincrotrone Trieste, S.S. 14 Km 163.5 in Area Science Park, 34149 Basovizza – Trieste, Italy.*

Contents

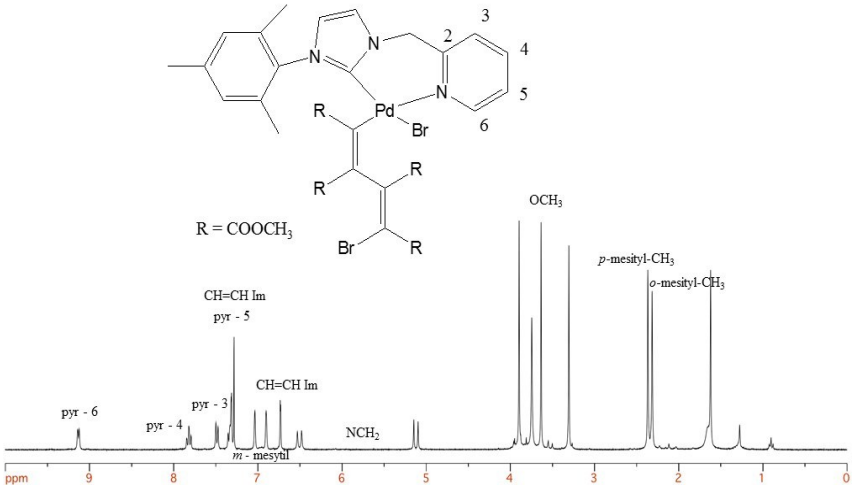

Fig. S1: ^{1}H NMR spectrum of complex **2b** in $CDCl_3$ at 298 K.

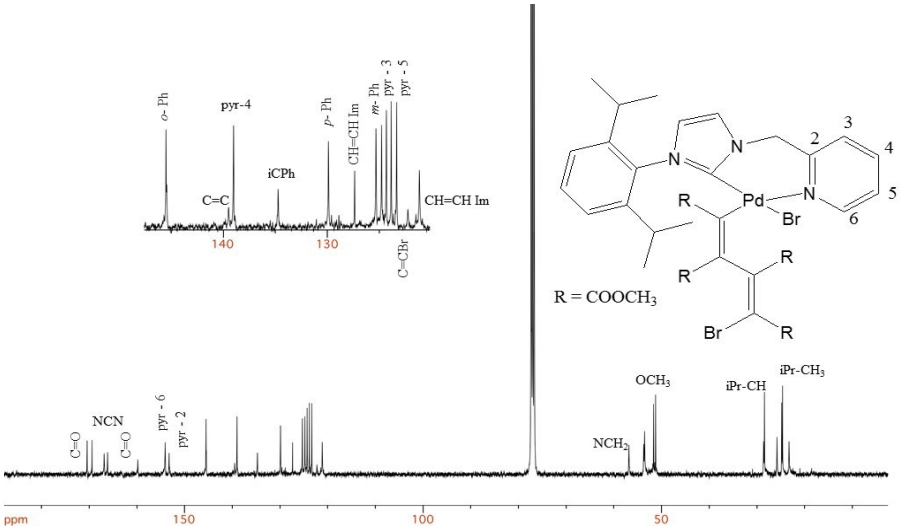

Fig S2: ^{13}C{^{1}H} NMR spectrum of the complex **2c** in $CDCl_3$ at 298 K.

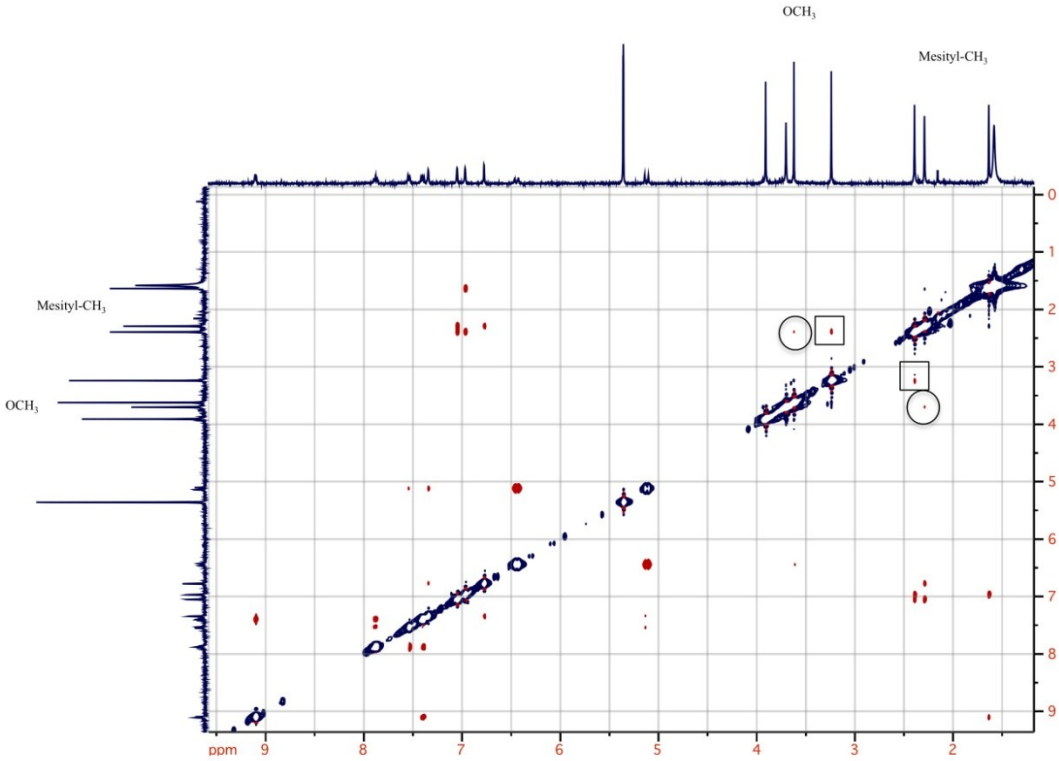

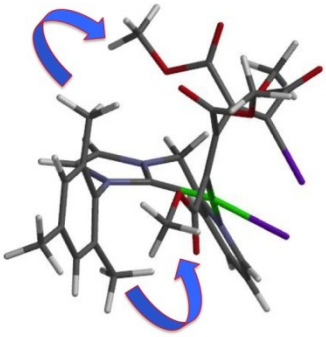

Fig S3 a: NOESY NMR spectrum of complex **2b** in CD_2Cl_2 at 298 K. The cross-peaks between the COOC<u>H</u>$_3$ protons of the butadienyl fragment and the o-methyl protons of mesityl substituent are highlighted by circles and squares.

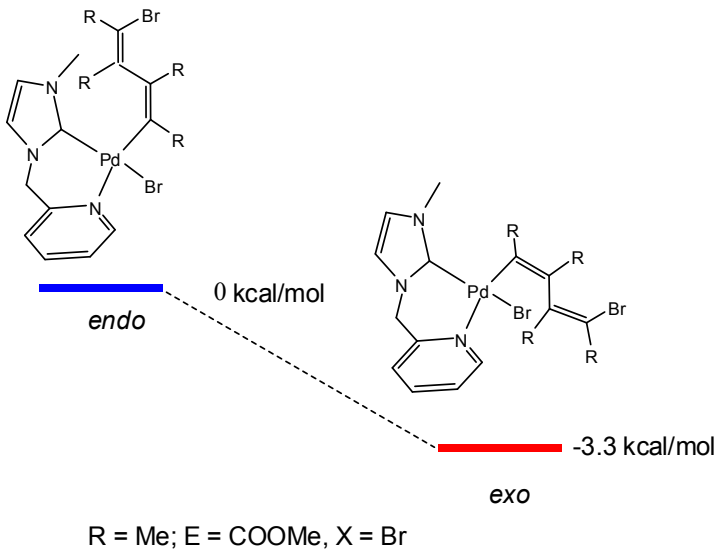

Fig. S3 b: Calculated energy (DFT) and topological representation of *endo* and *exo* isomers of complexes **2a**

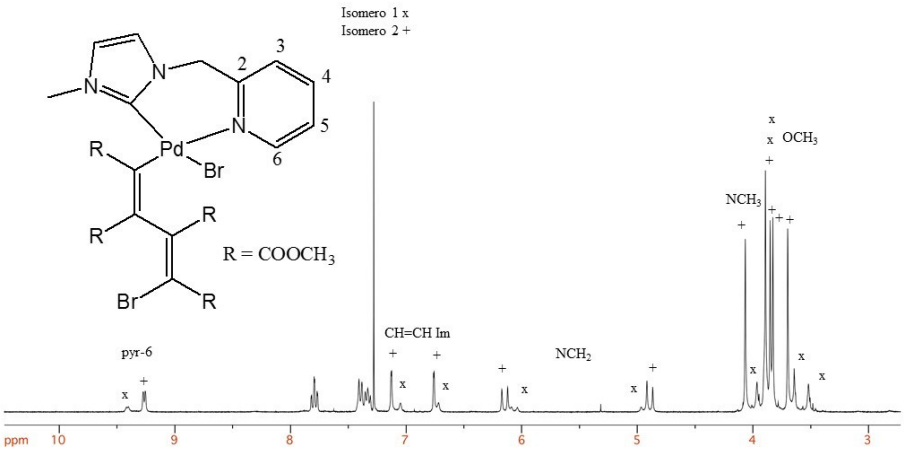

Fig. S3 c: ^{1}H NMR spectrum of complex **2a** in $CDCl_3$ at 298 K

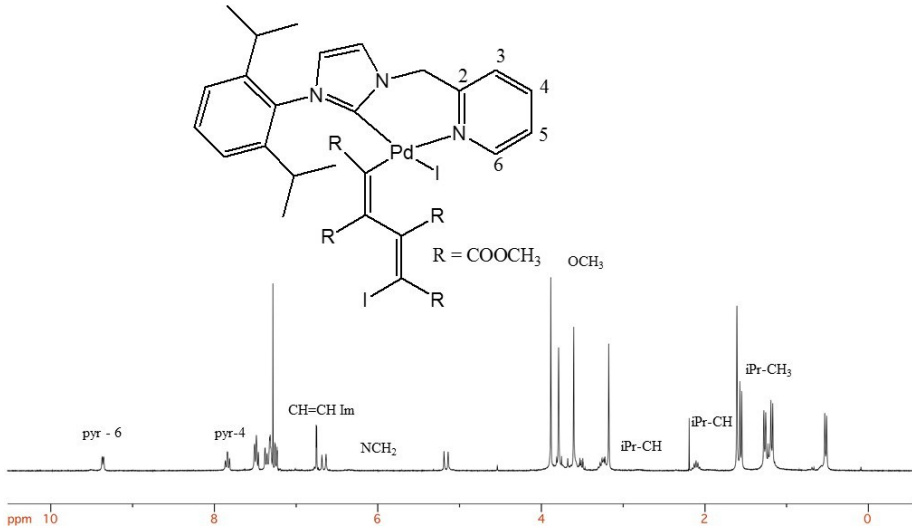

Fig. S4: ^{1}H NMR spectrum of complex **3c** in $CDCl_3$ at 298 K

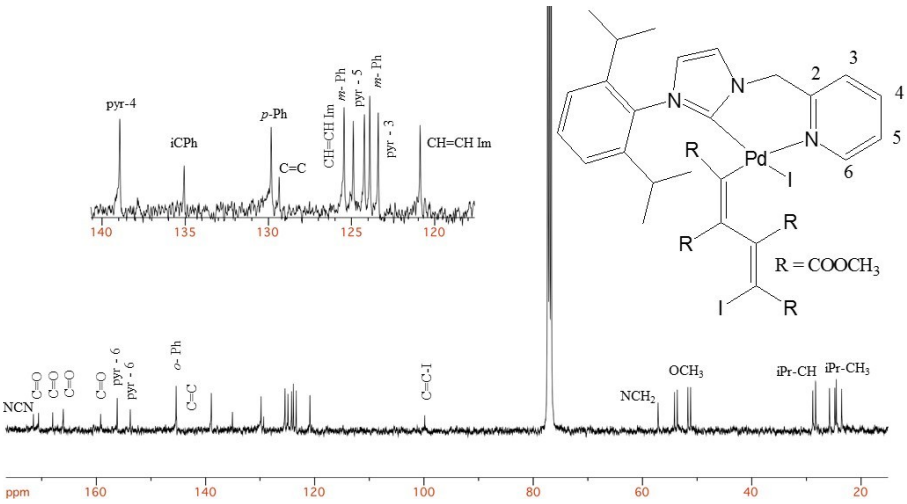

Fig S5: ^{13}C{^{1}H} NMR spectrum of the complex **3c** in $CDCl_3$ at 298 K.

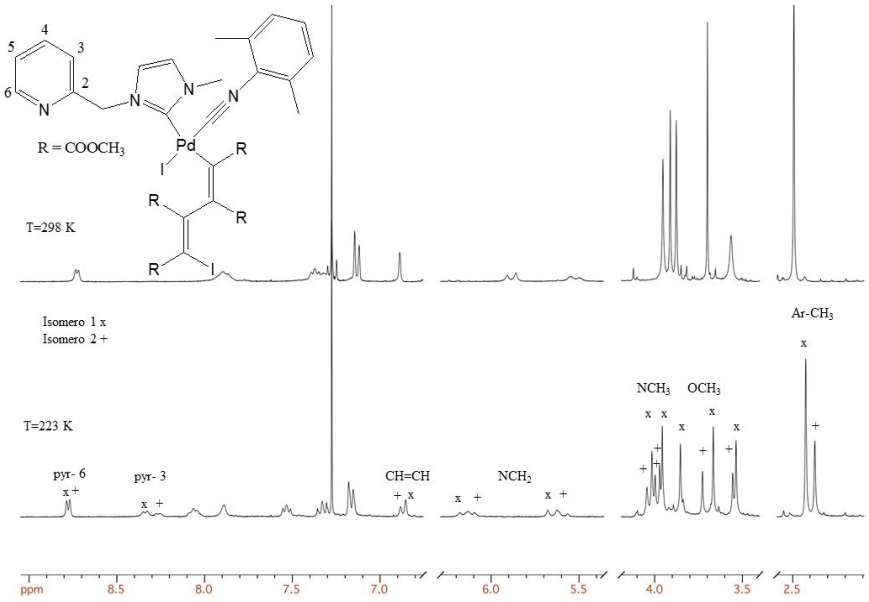

Fig. S6: ^{1}H NMR spectra of complex **3d** in $CDCl_3$ at 298 K (top) and 223 K (bottom)

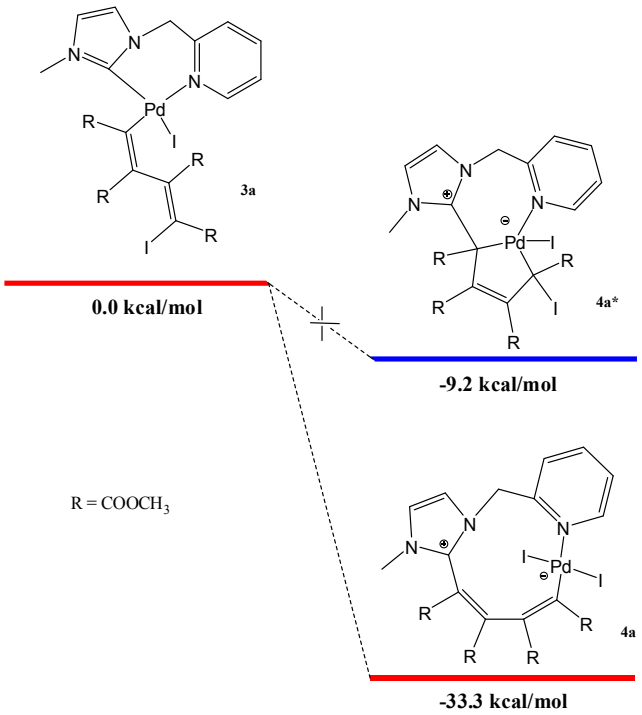

Fig. S7: Comparison among relative stabilization energy of the complexes **3a**, **4a*** and **4a**

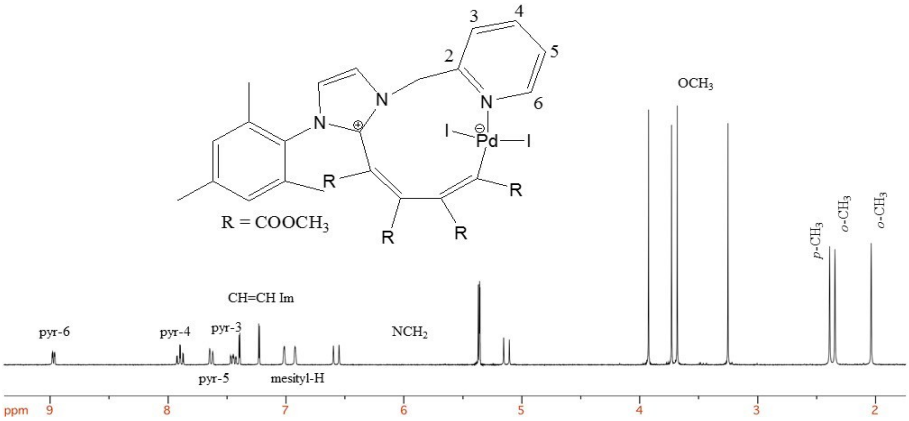

Fig. S8: a) ^{1}H NMR spectrum of complex **4b** in CD_2Cl_2 at 298K

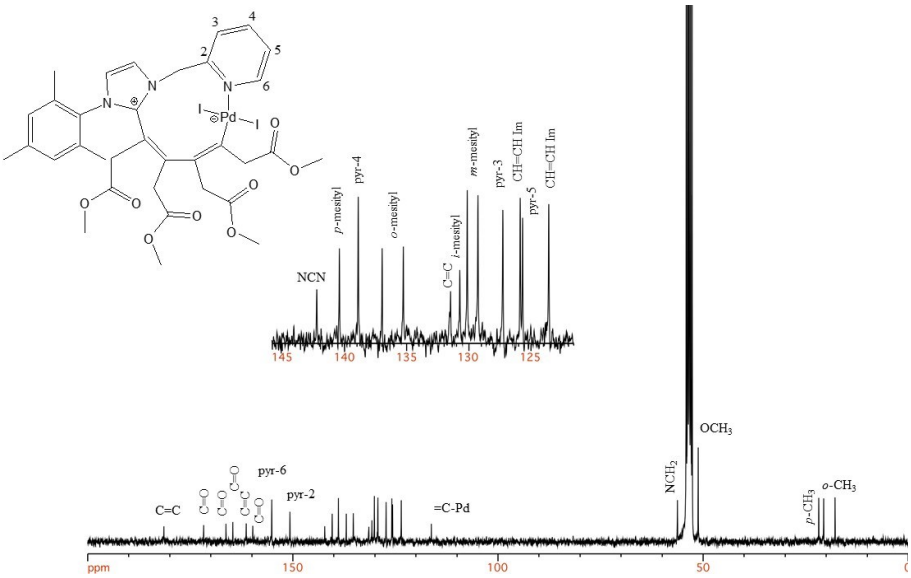

Fig. S8: b) $^{13}C\{^{1}H\}$ NMR spectrum of complex **4b** in CD_2Cl_2 at 298K

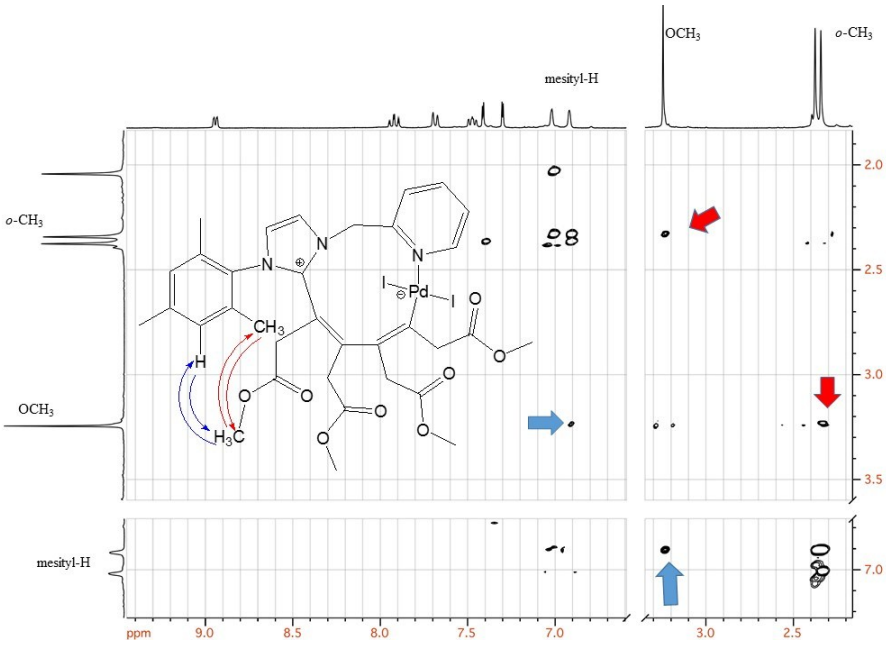

Fig. S8: c)NOESY ^{1}H NMR spectrum of complex **4b** in CD_2Cl_2 at 298K

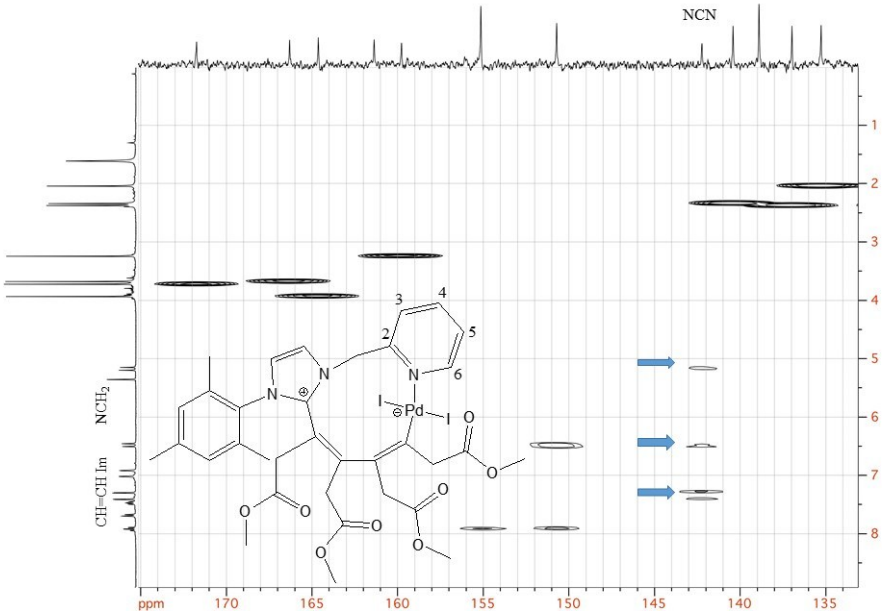

Fig S8: d) HMBC spectrum of complex **4b** in CD_2Cl_2 at 298K

Table S1: Crystallographic data and refinement details crystal forms of compound **4b**.

	Orthorhombic 4b	**Monoclinic 4b·¾CH_2Cl_2**
	$[PdC_{30}H_{31}I_2N_3O_8]$	$[PdC_{30}H_{31}I_2N_3O_8 \cdot 0.75CH_2Cl_2]$
CCDC Number	???????	???????

Chemical Formula	$PdC_{30}H_{31}I_2N_3O_8$	$PdC_{30.75}H_{32.5}Cl_{1.5}I_2N_3O_8$
Formula weight	921.78 g/mol	985.47 g/mol
Temperature	100(2) K	100(2) K
Wavelength	0.700 Å	0.700 Å
Crystal system	Orthorhombic	Monoclinic
Space Group	*P bca*	$P\ 2_1/c$
Unit cell dimensions	a = 19.777(4) Å	a = 10.929(2) Å
	b = 15.975(3) Å	b = 15.041(3) Å
	c = 20.563(4) Å	c = 21.431(4) Å
	α = 90°	α = 90°
	β = 90°	β = 94.00(3)°
	γ = 90°	γ = 90°
Volume	6497(2) $Å^3$	3514.3(12) $Å^3$
Z	8	4
Density (calculated)	1.885 $g\cdot cm^{-3}$	1.863 $g\cdot cm^{-3}$
Absorption coefficient	2.392 mm^{-1}	2.322 mm^{-1}
F(000)	3584	1918
Crystal size	0.08 x 0.02 x 0.02 mm^3	0.08 x 0.02 x 0.02 mm^3
Crystal habit	Dark yellow thin rods	Dark yellow thin rods
Theta range for data collection	1.89° to 27.04°	1.63° to 27.42°
Index ranges	$-25 \le h \le 25$,	$-14 \le h \le 14$,
	$-19 \le k \le 19$,	$-19 \le k \le 19$,
	$-26 \le l \le 26$	$-28 \le l \le 28$
Reflections collected	82101	52503
Independent reflections	7229, 6011 data with I>2σ(I)	8252, 7003 data with I>2σ(I)
Data multiplicity (max resltn)	10.54 (10.42)	2.57 (2.49)
I/σ(I) (max resltn)	25.88 (15.89)	10.89 (6.67)
R_{merge} (max resltn)	0.047 (0.104)	0.053 (0.101)
Data completeness (max resltn)	97% (95%)	99% (99%)
Refinement method	Full-matrix least-squares on F^2	Full-matrix least-squares on F^2
Data / restraints / parameters	7229/36/456	8252/6/443
Goodness-of-fit on F^2	1.047	1.045
Δ/σ_{max}	0.001	0.003
Final R indices [I>2σ(I)]	R_1 = 0.0426, wR_2 = 0.1080	R_1 = 0.0623, wR_2 = 0.1666
R indices (all data)	R_1 = 0.0525, wR_2 = 0.1157	R_1 = 0.0715, wR_2 = 0.1755
Largest diff. peak and hole	2.487 and -1.424 $eÅ^{-3}$	2.352 and -1.955 $eÅ^{-3}$
R.M.S. deviation from mean	0.157 $eÅ^{-3}$	0.217 $eÅ^{-3}$

$R_1 = \Sigma\ ||Fo|-|Fc|| / \Sigma\ |Fo|$, $wR_2 = \{\Sigma\ [w(Fo^2 - Fc^2)^2] / \Sigma\ [w(Fo^2)^2]\}^{½}$

Fig. S9:a) Ellipsoid representation of **4b** crystals ASU contents (50% probability): A) orthorhombic crystal form; B) monoclinic crystal form; C) naming scheme adopted for both crystal structures.

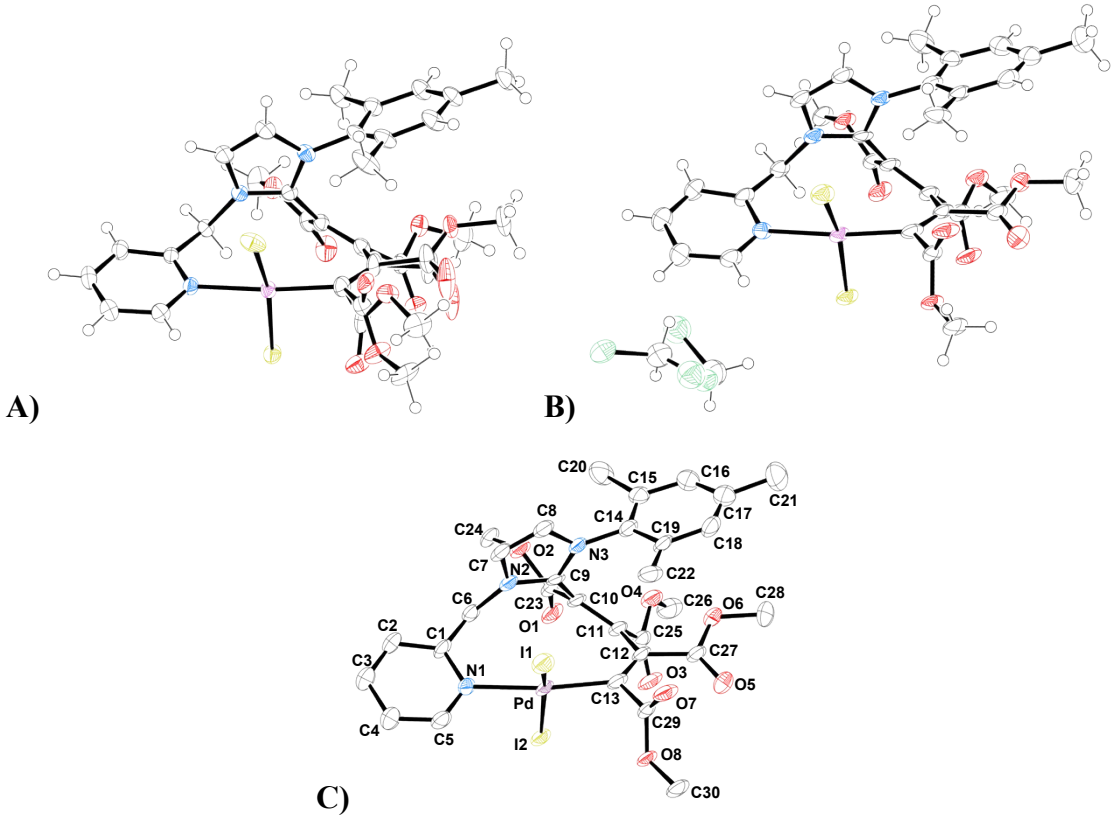

b) Superimposition of **4b** conformations found in orthorhombic (light green sticks) and monoclinic (grey sticks) crystal forms. R.m.s. deviation between overlapped atoms equal to 0.65 Å.

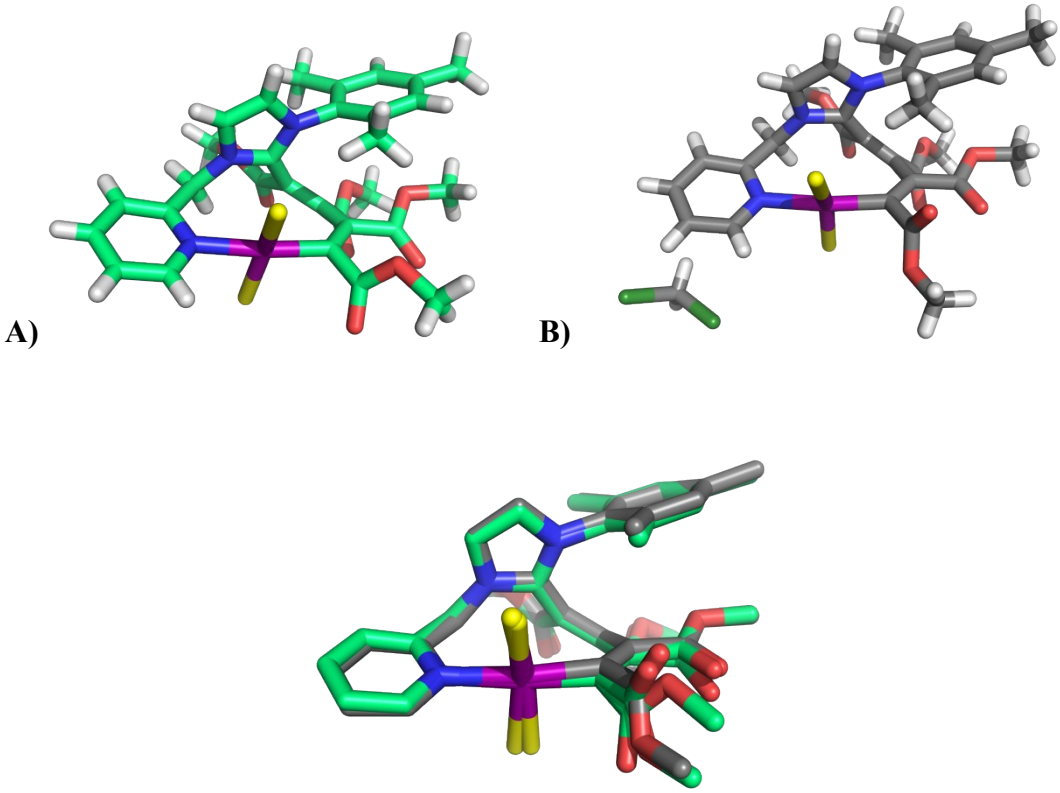

Fig. S10. Ortep representation of complex **4b** and **4bsolv**.*

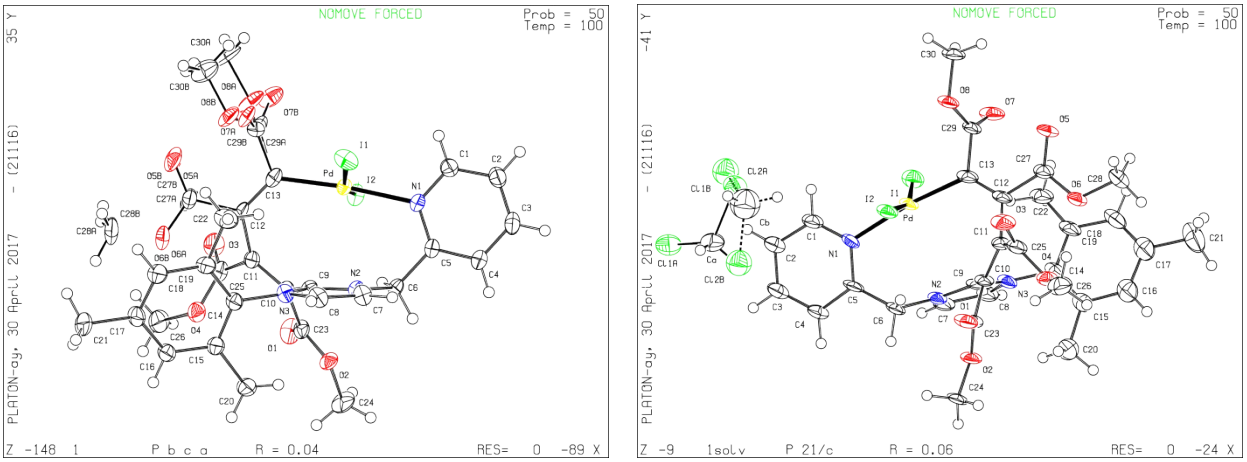

* L. Farrugia, *Journal of Applied Crystallography*, 2012, **45(4)**, 849-854.

Fig. S11 a-j: NMR spectra of the complexes not mentioned in the text.

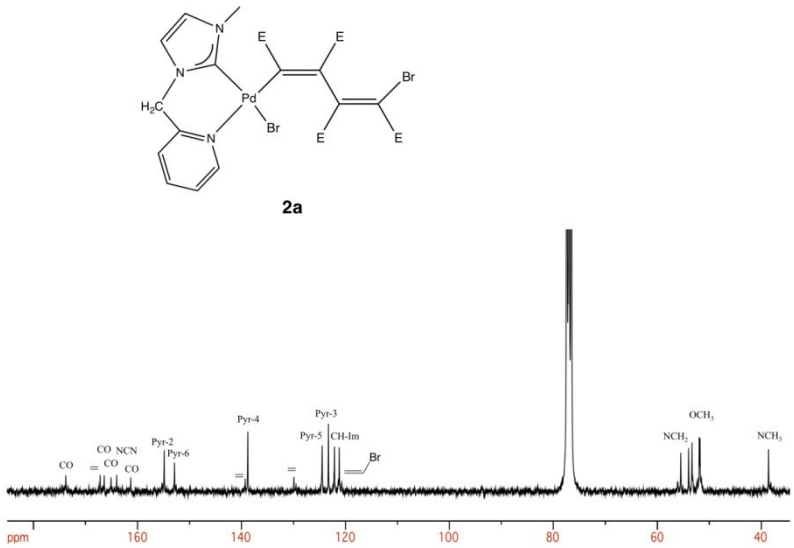

Fig S11 a: $^{13}C\{^{1}H\}$NMR spectrum of the complex **2a** in $CDCl_3$ at 298 K (E = COOMe)

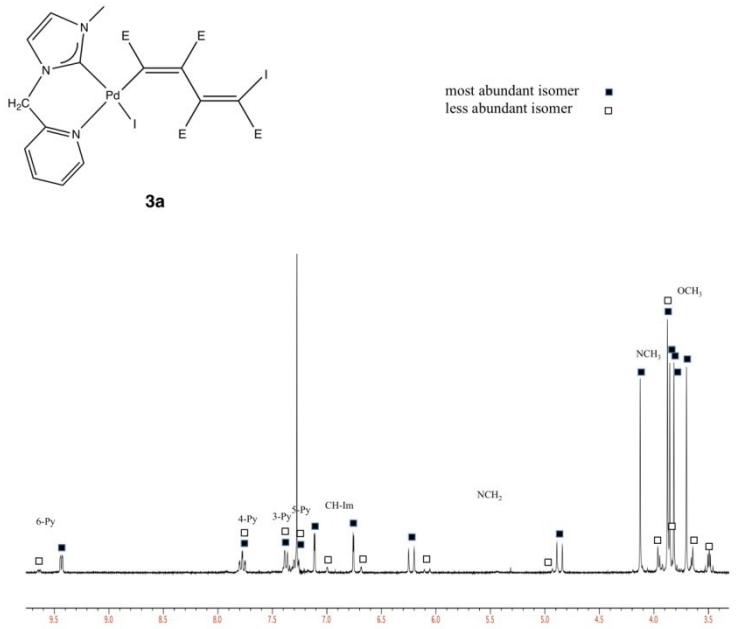

Fig S11 b: ^{1}H NMR spectrum of the complex **3a** in $CDCl_3$ at 298 K (E = COOMe)

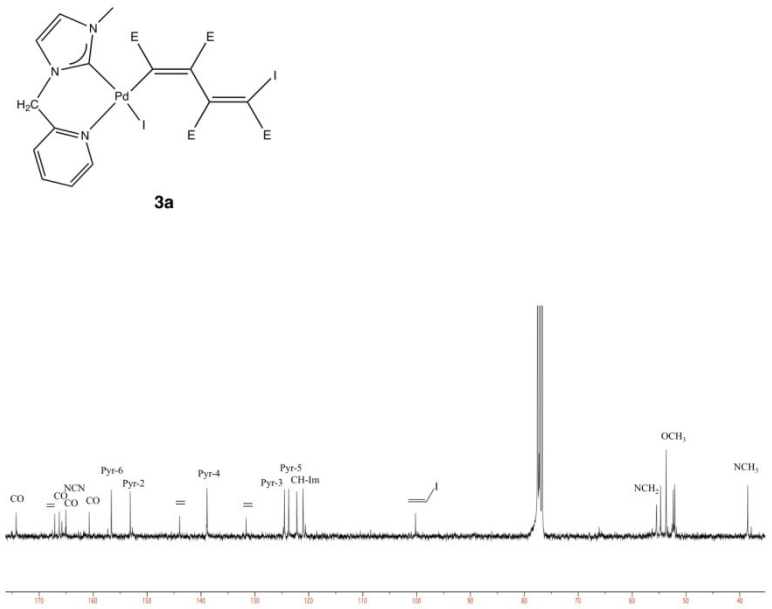

Fig S11 c: $^{13}C\{^{1}H\}$ NMR spectrum of the complex **3a** in $CDCl_3$ at 253 K (E = COOMe)

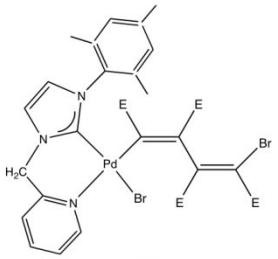

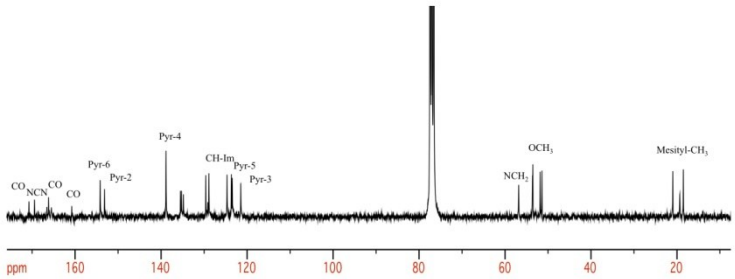

Fig S11 d: $^{13}C\{^{1}H\}$ NMR spectrum of the complex **2b** in $CDCl_3$ at 298 K (E = COOMe)

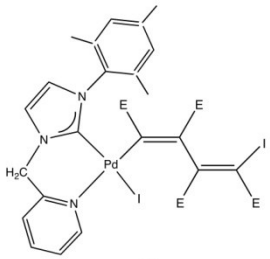

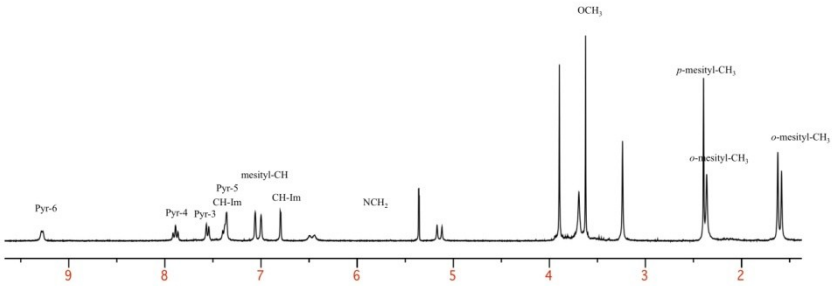

Fig S11 e: ^{1}H NMR spectrum of the complex **3b** in CD_2Cl_2 at 298 K (E = COOMe)

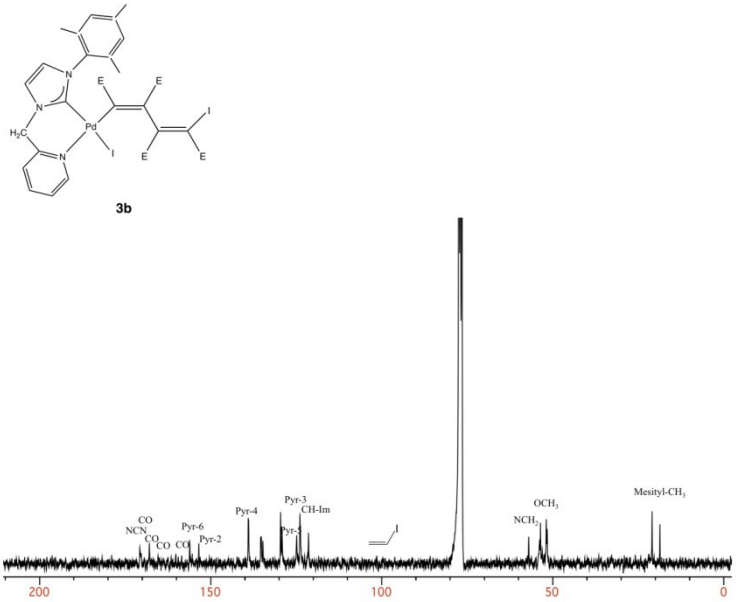

Fig S11 f: $^{13}C\{^{1}H\}$ NMR spectrum of the complex **3b** in $CDCl_3$ at 298 K (E = COOMe)

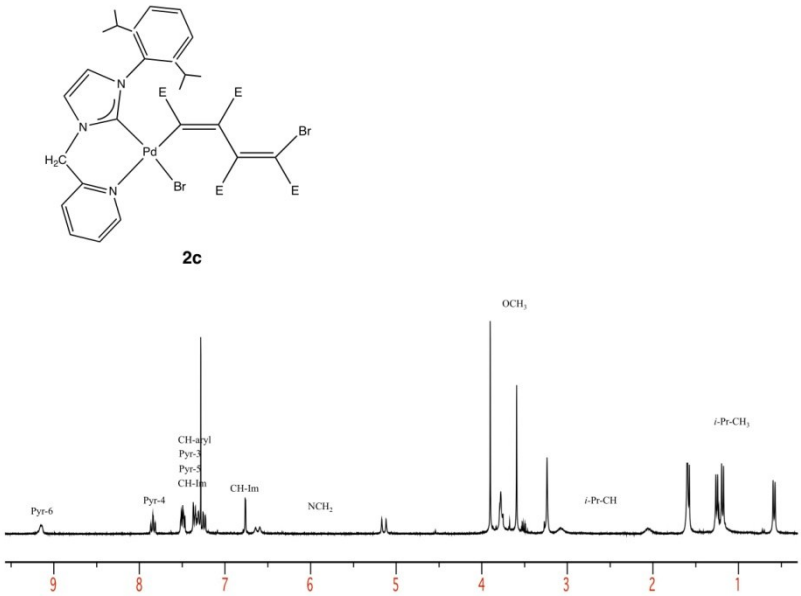

Fig S11 g: ^{1}H NMR spectrum of the complex **2c** in $CDCl_3$ at 298 K (E = COOMe)

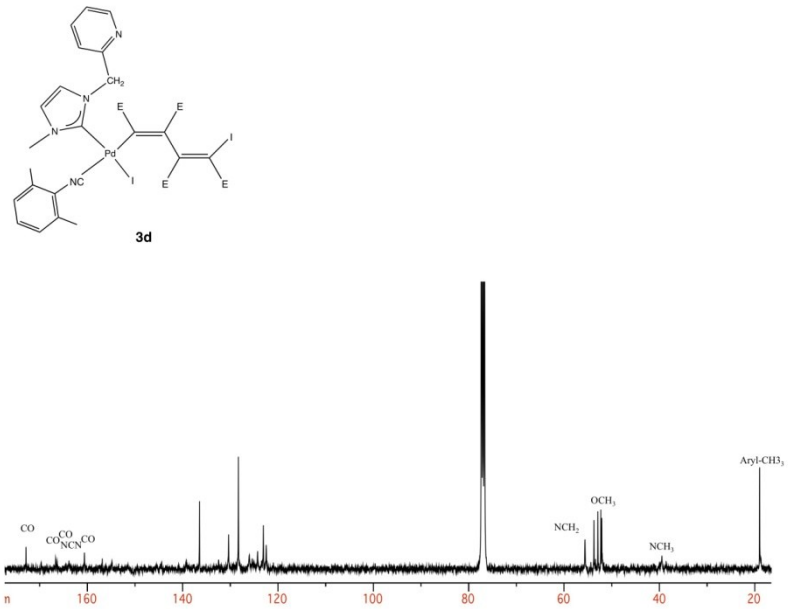

Fig S11 h: $^{13}C\{^{1}H\}$ NMR spectrum of the complex **3d** in $CDCl_3$ at 298 K (E = COOMe)

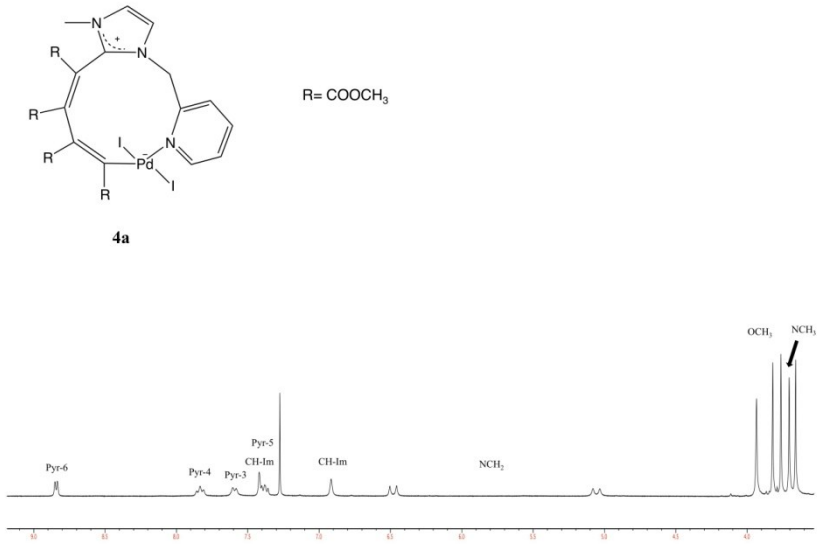

Fig S11 i: ^{1}H NMR spectrum of the complex **4a** in $CDCl_3$ at 298 K

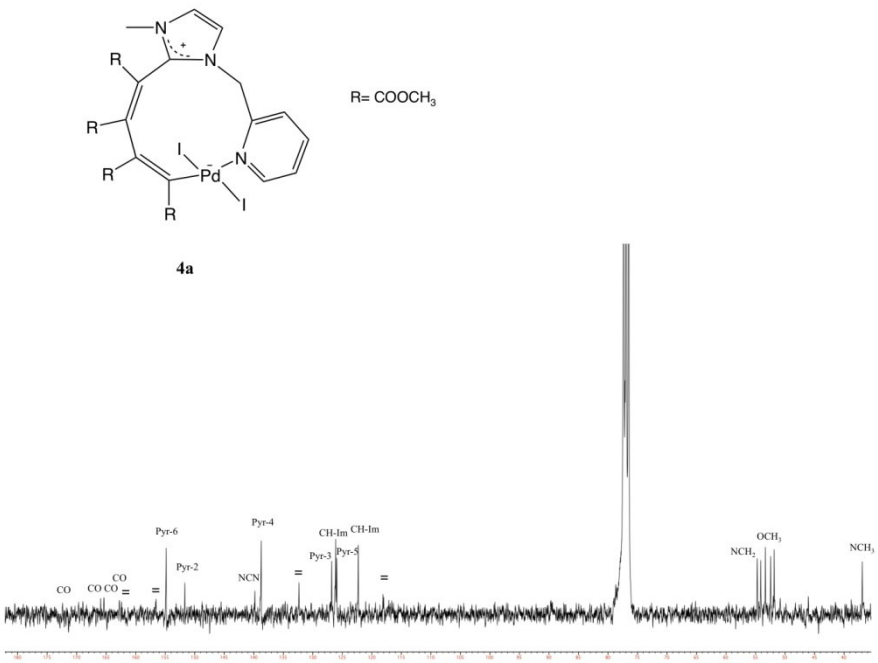

Fig S11 j: $^{13}C\{^{1}H\}$ NMR spectrum of the complex **4z** in $CDCl_3$ at 298 K